Probing the densities of Sn isotopes

K. Amos* and S. Karataglidis†
School of Physics, University of Melbourne, Victoria 3010, Australia

J. Dobaczewski‡
Institute of Theoretical Physics, Warsaw University, PL-00-681, Warsaw, Poland
(Received 19 February 2004; published 31 August 2004)

Proton and neutron densities have been obtained for the even–even isotopes of Sn from ^{100}Sn to ^{176}Sn using a Hartree-Fock-Bogoliubov model with a Skyrme interaction. The matter densities so defined have been used with realistic nucleon–nucleon interactions in a folding model to specify optical potentials for the elastic scattering of protons with energies in the range 40–200 MeV. Those potentials have been used to make predictions of the differential cross sections and spin observables for proton scattering. As the target mass increases, the emergence of the neutron skin in the Sn isotopes is revealed by marked effects in the differential cross section. Comparisons with available data show how similar scattering data for the neutron-rich isotopes may provide constraints for the model structures.

DOI: 10.1103/PhysRevC.70.024607 PACS number(s): 25.40.Cm, 21.10.Gv, 24.10.Ht

I. INTRODUCTION

One of the goals of modern nuclear physics is to understand the structures of nuclei far from the line of stability and at extremes of isospin. Thus far studies have largely dealt with the light nuclei for which radioactive beams have been available at facilities such as TRIUMF/ISAC, NSCL, RIKEN, and CERN/ISOLDE. Prior experiments have led to the identification of structures of which the halo [1] is the best known after its identification in ^{11}Li. In light of projected experimental facilities using radioactive ion beams to extend such investigations to heavy nuclei, there have been advances in the theoretical study of neutron rich nuclei across the whole mass range (see Refs. [1–5] for reviews). Studies of so-called exotic nuclei have topical interest since nuclei far from stability play an important role in stellar nucleosynthesis with short-lived species formed as part of the *r*– and *rp*– processes. Notably the structure of such nuclei determine the rates at which α– and nucleon–capture reactions proceed against the interplay of weak decays and photodisintegration; key elements in the determination of the abundances of nuclei in the universe.

Of course, these exotic systems are of interest in their own right given that they may exhibit forms of nuclear matter quite different from those of stable isotopes. Of particular interest are the separate density distributions of proton and neutrons. As well as halos, heavier systems may lead to the identification of pronounced neutron skins [6] and/or to dramatic changes in nuclear shell structure [7].

An important quantity by which the model structures are tested is the ground state density. For stable nuclei, one usually seeks information about that from the elastic scattering of electrons. The electron scattering form factors so determined are measures of the charge and current densities of the nucleus. Complementing that information, which primarily focuses on the proton density itself, are analyses of data from the elastic scattering of nucleons. Nucleon scattering probes the matter density of the nucleus and, at the energies we consider, of the neutron matter distribution in particular since the effective nucleon–nucleon (NN) interaction is strongest in the isoscalar $^3S_1$ channel [8]. Of course, there are non-negligible contributions to proton scattering from their interactions with the bound protons and such are included in all calculations we have made. But as evident from the recent study [9] of proton and neutron elastic scattering at the same energies from ^{208}Pb, the differential cross sections from proton (neutron) scattering reflect changes primarily made in the distributions of neutron (proton) matter distributions of the target. Indeed they did so sufficiently well that cross-section data could be used to estimate the neutron skin thickness of ^{208}Pb. For radioactive nuclei, the only available equivalent measure of the ground state density comes from the scattering of those nuclei from hydrogen which, in inverse kinematics, corresponds to proton scattering from the nucleus as target.

For nuclei above the *fp*-shell, mean-field models of structure are at the forefront of current studies of the ground state densities. Usually those calculations are made in a relativistic Hartree or Hartree-Fock model [10–14] or a nonrelativistic Skyrme-Hartree-Fock-Bogoliubov model [15–18]. This mean-field approach works as the ground state properties for heavy nuclei arise more generally from the bulk properties of the density as opposed to single particle properties. As one approaches the drip lines however, surface properties become more important and, in concert, so do single particle densities.

As noted above, a test case has been to use nucleon elastic scattering to determine/extract the neutron skin thickness in ^{208}Pb. Karataglidis *et al.* [9] have shown that the differential cross sections from the elastic scattering of 200 MeV protons from ^{208}Pb suggests a neutron skin thickness in ^{208}Pb of

*Electronic address: amos@physics.unimelb.edu.au
†Electronic address: kara@physics.unimelb.edu.au
‡Electronic address: Jacek.Dobaczewski@fuw.edu.pl

 ©2004 The American Physical Society

$\sim$0.17 fm; a result that has been confirmed recently [19]. More importantly, the study by Karataglidis *et al.* [9] also showed that such scattering analyses could select between disparate model structures that have the same root mean square (rms) radii. By itself, the rms radius is not an adequate indicator of the validity of a model structure. To use the scattering data to differentiate between models of structure, a predictive theory of nucleon–nucleus (*NA*) scattering was needed, and such has been developed in the past decade [8]. That theory is *direct* in that all quantities required are defined *a priori* with no *a posteriori* adjustment of results. With the nucleus viewed as a system of *A* nucleons, *NA* scattering is determined by an optical potential formed by a folding process. Such microscopic approaches defining the *NA* optical potential have been quite successful in predicting both angle-dependent and integral observables of elastic scattering [8,20]. It is important to note that distinction in scattering cross sections resulting from use of different "sensible" models of structure are in the details, and particularly with results in the region of $1-2.5$ fm^{-1} momentum transfer values. Thus one needs as complete a calculation of the optical potentials as possible and if feasible to use them with no further approximation. The contribution to scattering of the knockout exchange amplitudes for all energies are such that it is not wise to use an equivalent localization of the associated nonlocal terms. We do not and so we solve the nonlocal Schrödinger equations directly. However, that also means we must have single particle bound state wave functions (or equivalently the complete one body density matrix elements) and not just the matter densities from structure.

The Sn isotopes are of interest for current structure studies. Many of the sets which span the quite extensive range of mass between the nucleon drip lines can be formed as radioactive ions with some in numbers sufficient to perform scattering experiments. Measurements of proton scattering from ^{114,116,118,120,122,124}Sn have been reported for many energies and most recently at an energy of 295 A MeV [21,22]. Using a relativistic impulse approximation with model (sum of Gaussians) matter densities, analyses [22] of the 295 MeV (preliminary) data indicated [22] that the isotopes from mass 120 on had a noticeable effect from neutron occupancies of the $3s_{1/2}$ shell. Their analyses also indicated that scattering data revealed a gradual change in neutron densities as the mass of the isotope increased. Matching the data needed inclusion of nuclear medium effects on the (NN) coupling constants and exchanged meson masses altering them from those of free NN scattering. Not only are those data preliminary, but the energy is on the high side of the range for which we are confident that our current nonrelativistic, *g*-folding method of defining optical potentials microscopically is valid. Notably we believe that the method by which we define effective NN interactions at and above 295 MeV may need correction. Thus we have made calculations of scattering of protons from many Sn isotopes at lower energies using the program DWBA98 [23] that forms *g*-folding optical potentials [8]. The same program then solves the associated nonlocal Schrödinger equations. Specifically we have calculated cross sections for the scattering of all the even mass isotopes $^{100-176}$Sn from hydrogen at an energy of 200 A MeV, and for lower energies, from those isotopes for which data exist.

The relevant optical potentials were formed by folding realistic effective NN interactions with the details of densities of those nuclei given by the mean-field models of their structure. With optical potentials so formed previously, differential cross sections and spin observables for proton scattering (and at 200 MeV in particular) from diverse targets ranging from ^{3}He to ^{238}U have been predicted and found to agree very well with data; providing that the structure with which the effective NN interactions are folded is appropriate. The NN effective interactions were determined from NN *g* matrices (solutions of Brueckner-Bethe-Goldstone equations for nuclear matter) found from realistic free NN forces. Details of the specifications of those effective NN interactions, of the folding process that gives the optical potential, and of the successful predictions of differential cross sections and analyzing powers from the scattering of protons at diverse energies and from diverse mass targets, have been summarized before [8] and so are not repeated herein. However, of note is that with confidence in the chosen effective NN interactions and in the applicability of the *g*-folding method, the evaluations when compared with data serve as a test of the putative model structures. Hence, a priamary purpose of these studies has been to note characteristics in scattering predictions linked to isotope change in the Sn nuclei if they are described appropriately by the Hartree-Fock-Bogoliubov model with a Skyrme interaction. Of course, only access to appropriate data will allow any critique on the specific mean-field structures of the Sn isotopes.

In summary, our purpose in this paper is to investigate the ways in which proton elastic scattering data may reflect attributes of matter distributions, and especially of the neutron distribution, as one varies from the proton to the neutron drip line in the mass table. We consider the even mass (and so $J=0$) Sn isotopes since there are many of them and because we have structure models for them that may well be credible descriptions. However, even if some isotopes are not so well described, when experiments can be made, the differences between measurement and our predictions help to find the more relevant matter description.

In Sec. II, we outline the structure models used in our scattering calculations and present details of the resulting proton and neutron matter distributions. In Sec. IV we show the results found using those structures and an established effective NN force in nuclear matter in generating *g*-folding optical potentials for a wide range of Sn isotopes scattering from hydrogen. An energy of 200 A MeV has been used. In Sec. V application of structure and scattering models is made for a number of cases for which proton elastic scattering data are available. Conclusions are presented in Sec. VI.

II. MODELS OF STRUCTURE OF THE Sn ISOTOPES

In the present study, the properties of even–even Sn isotopes (masses 100–176) are described using the spherical mean-field Hartree-Fock-Bogoliubov model [15]. Two Skyrme interactions have been used. As details of the method have been given in detail elsewhere [17,24,25], only features pertaining to the particular calculations discussed are given. We have used two parameterizations of the

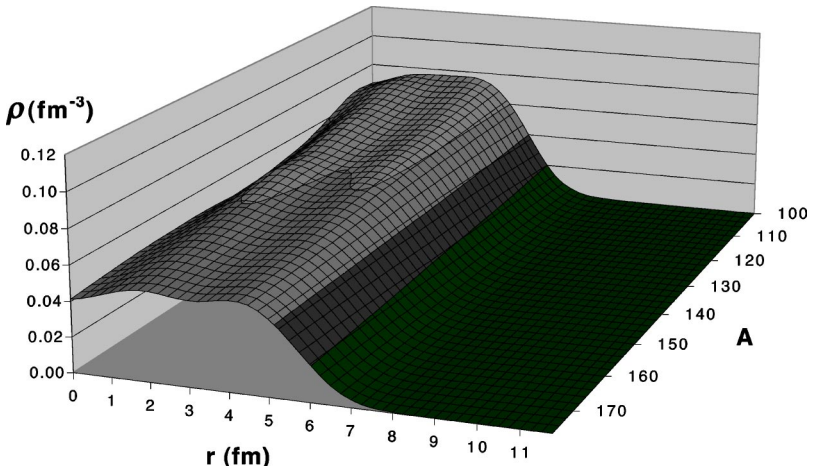

FIG. 1. The proton density variation with mass number from the SLy4 model of structure for the Sn isotopes.

Skyrme force, SkP [24] and SLy4 [26], which in the past have given appropriate descriptions of bulk nuclear properties. They differ by the input values of the nuclear-matter effective mass, being $m^*/m=1$ and 0.7, respectively. The zero-range density-dependent pairing force was used in the particle-particle channel and with the form that is intermediate between volume and surface attraction [17]. A large positive energy phase space of 60 MeV was taken for which the pairing-force strengths of $V_0=-286.20$ and -212.94 MeV fm^{-3} were obtained in the SkP and SLy4 cases, respectively. Those strengths result from using a standard adjustment [27] of the neutron pairing gap in ^{120}Sn.

Both model structures agree well with the two-neutron separation energies S_{2N} and neutron pairing gaps Δ_N extracted from data from even mass Sn isotopes having neutron numbers between the magic numbers $N=50$ and $N=82$. At the magic numbers, the calculated gaps vanish due to the known effect of an unphysical, too sudden, pairing phase transition. The size of the jump of S_{2N} at $N=82$ is slightly underestimated (overestimated) by the SkP (SLy4) model which is an effect of the different values of the effective mass. Nevertheless, the overall quality of agreement between theory and experiment suffices for us to consider the two models to be useful for extrapolations to describe unknown heavy Sn isotopes. Within the two models, the heaviest two-neutron-bound isotope is predicted to be mass 172(174) for SkP(SLy4).

Spatial properties of neutron and proton density distributions are of special interest in a number of contexts. In the form of one body density matrix elements (OBDME), which we define later, and the nucleon single particle wave functions, they are central aspects of a predictive method of calculating their scattering from hydrogen targets. Of course, geometric aspects of nuclei, and of the Sn isotopes in particular, have been found in the past [6]. Often they have been defined by using the Helm model and the locations of maxima and minima of associated form factors. Also bulk density values sometimes have been assessed from averaging density functions from the structure models. Therefore, care must be exercised in equating radii and other bulk properties of the same nucleus from different studies to ensure that they refer to the same quantity. Trends of geometries with mass may be equated.

With an increasing number of neutrons, from the past [6] as well as these studies, the neutron and proton radii of the Sn isotopes increase at different rates with the neutron radii increasing faster. As a result there is a gradual increase in the size of the neutron skin; an increase that is almost linear with neutron number. At the same time the neutron and proton bulk densities increase and decrease, respectively. The balance between the bulk and surface increase of the neutron distribution is governed by the volume and surface attractions between neutrons and protons and hence is fixed by the principal features of the volume and surface terms in nuclear

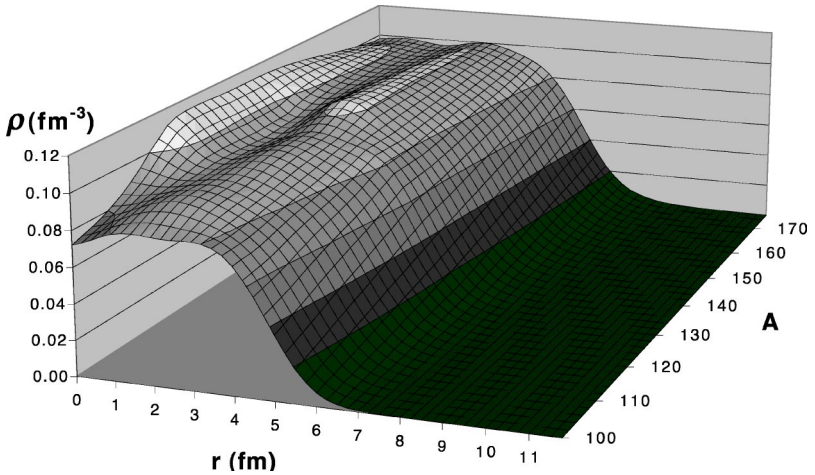

FIG. 2. The neutron density variation with mass number from the SLy4 model of structure for the Sn isotopes.

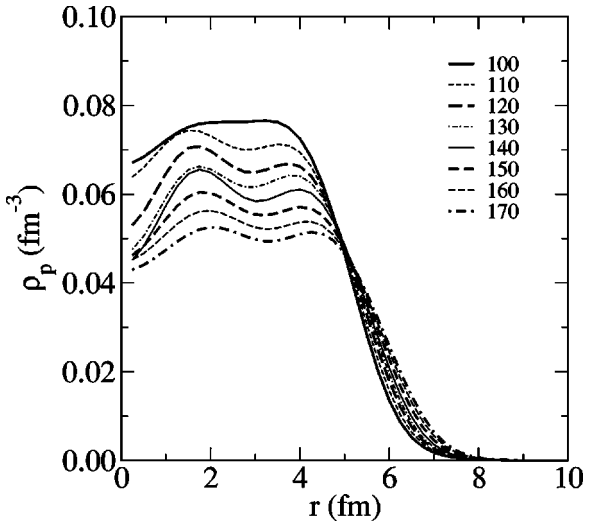

FIG. 3. The proton densities given by the SkP model of structure for eight isotopes of Sn.

masses. That is evident from the actual density profiles deduced from the shell occupancies and associated canonical wave functions of the mean-field model results. Such complete density distributions for all of the even mass Sn isotopes resulting from the SLy4 and SkP models of their structure are so shown in Figs. 1–4. The normalization of the neutron densities we show is

$$4\pi\int_0^\infty \rho_n(r)r^2dr = N. \tag{1}$$

There is a similar form for the protons.

Using the SLy4 force, the proton and neutron matter distributions for all even mass Sn isotopes resulting from the mean-field calculations are displayed in Figs. 1 and 2, respectively. The proton (neutron) distributions are plotted with nuclear mass decreasing (increasing) into the page. By

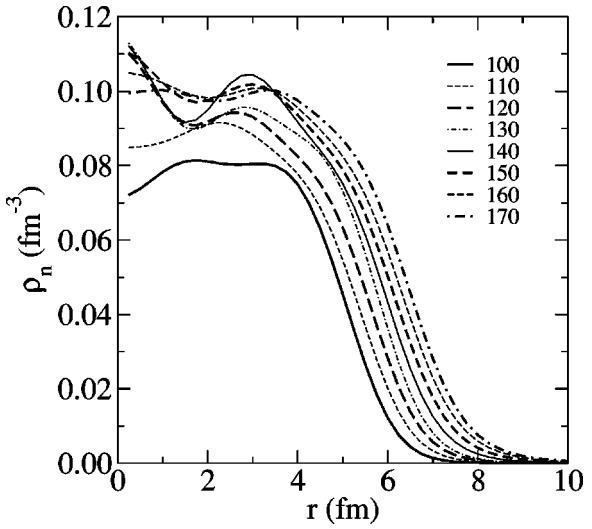

FIG. 4. The neutron densities given by the SkP model of structure for eight isotopes of Sn.

TABLE I. Surface characteristic values of the proton distributions shown in Fig. 3.

Isotope	ρ_{bulk} (fm^{-3})	$(\Delta r)_{90-10}$ (fm)	Slope (fm^{-2})
100	0.076	2.07	−0.036
110	0.071	2.09	−0.032
120	0.068	2.10	−0.031
130	0.066	2.05	−0.029
140	0.063	2.05	−0.027
150	0.057	2.10	−0.027
160	0.054	2.10	−0.021
170	0.050	2.02	−0.018

that means the variations to those densities are best portrayed in block form. In these figures we display lines of equal radii and use different shadings to designate regions over which the density changes by 0.02 fm^{-3}. The proton number of course is fixed at 50 and so as the neutron number increases, and concomitantly the neutron volume increases, those 50 protons extend over an increasing volume. As noted above that is due to the strong attractive neutron–proton interactions. In concert, the central charge density must, and does, decrease. However, and as will be seen more clearly in Fig. 3 below, the charge distributions do not become significantly more diffuse. The prime effect is the ~33% increase in the charge volume.

The neutron densities structure variation with increasing mass is quite different from that of the protons. Such is not unexpected as the proton number is fixed at 50 with the neutron number increasing to give the mass range. The general trend that the neutron rms radii increase is evident as the half central density is reached at radii ranging from ~5 fm in ^{100}Sn to ~6.5 fm for ^{170}Sn. The increase of the neutron surface radius is observed readily in this figure by noting the changes along the lines of fixed radius. We note also that a strong oscillation develops in the central density, which on average also increases from ~0.08 neutrons/fm^3 in ^{100}Sn to ~0.1 neutrons/fm^3 for ^{170}Sn.

The mass variations of densities are evident also in Figs. 3 and 4 wherein the proton and neutron densities, respectively, for the Sn isotopes calculated using the SkP model are given for a select set of eight nuclei having masses spaced evenly between 100 and 170. With the SLy4 force the mass trends are very similar with differences occurring in fine details.

While a few of these densities have been depicted before [6] not only do we extend the set to a wider mass range and fill in previous gaps but we highlight features that should most readily relate to effects in predictions of scattering. In Fig. 3 it is evident that the 50 protons are rearranged to be more extensive as one increases mass. Note that the half-density radius ranges from ~5 fm for ^{100}Sn to ~6 fm in ^{170}Sn. However the proton surface diffuseness, the distance over which the charge density falls from 90% to 10% of its central value, does not vary greatly over the set of nuclei. The slope of the densities do change as is obvious in the figure. Those two properties are listed in Table I. The diffuseness is somewhat subjective in that the internal densities are

structured. That is especially so at the center and so we had to make a reasonable guess at an internal value from which to define the 90% and 10% radii. Those guess values are also listed. The slopes though are quite well given by the variation around 5.5 fm for the heavier isotopes and around 5.0 fm for the lighter ones. From the values listed, the surface diffuseness of the proton distributions for these isotopes do not vary greatly and may be taken as 2.07 ± 0.05 fm. To attain that there has to be the steady progression of the slopes of those surfaces; understandable as the stretching of the distribution of the 50 protons as neutrons are added mostly in the surface region to form heavier isotopes.

By inspection of Fig. 4, the neutron distributions also have surface diffuseness values of ~ 2 fm. Thus there is a gradual development of a neutron skin to the Sn isotopes, for while with ^{100}Sn the 50 protons and 50 neutrons have essentially the same distribution (solid dark lines in the figures), the two density profiles are somewhat disparate in ^{170}Sn. Not only does the neutron central density increase by $\sim 25\%$ from its value in ^{100}Sn while the proton central density value decreases by $\sim 40\%$, but the skin, in this case $R_{\rm rms}(\text{neutron}) - R_{\rm rms}(\text{proton})$, varies from 0 to ~ 0.5 fm as noted previously from the definition in the Helm model characterization [6].

It is of note also that the neutron density profiles have a mass variation through the inner region (~ 4 fm) that is not as smooth a progression as that in the outer radial region (beyond 4 fm). Those changes in shape for masses in the vicinity of 150 we expect to reflect as variations in cross section properties for momentum transfer values $1-2$ fm^{-1} (at least for 200 MeV scattering) as such did for analyses of data from 200 MeV proton scattering from ^{208}Pb [9].

III. MASS VARIATION OF SINGLE PARTICLE LEVEL PROPERTIES

A. The protons in the Sn isotopes

To a very high degree, the SLy4 and SkP models give the same closed orbit proton configuration for the 50 protons in all of the Sn isotopes, i.e.,

$$(0s_{1/2})^2(0p_{3/2})^4(0p_{1/2})^2(0d_{5/2})^6(1s_{1/2})^2(0d_{3/2})^4 \times (0f_{7/2})^8(1p_{3/2})^4(0f_{5/2})^6(1p_{1/2})^2(0g_{9/2})^{10}. \quad (2)$$

However, the associated single proton wave functions vary with the mass of the isotope reflecting the expected expansion of the charge density as the neutron numbers, and in concert the nuclear skin, increases. That variation is depicted in Fig. 5. Therein are shown the changes that occur over the mass range in the modulus square of the $0s_{1/2}$, the most bound of single particle states, and in that of the $0g_{9/2}$ orbit, the latter being a dominant element in defining the charge properties near and in the nuclear surface. Clearly these wave functions extend as the neutron number increases, as do those of all of the other occupied orbitals. But since the number of protons is fixed at 50, the charge density then gradually decreases in the nuclear center while at long range the density gradient at the surface decreases in size. This behavior, which is in stark contrast to that of the neutron density, should be clearly evident if ever longitudinal form factors of these isotopes from electron scattering can be measured.

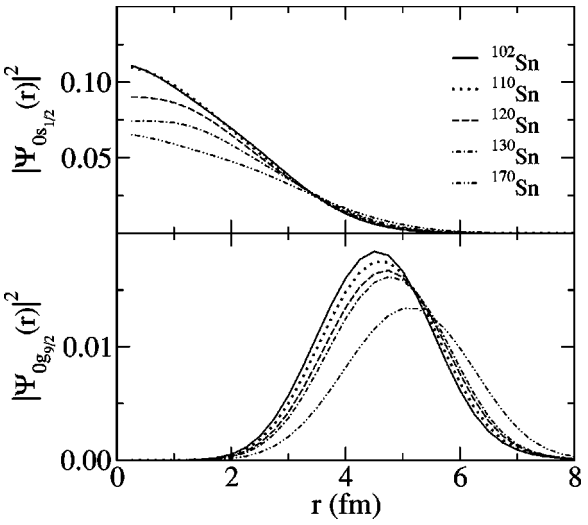

FIG. 5. The moduli square of the radial functions for the $0s_{1/2}$ (top) and $0g_{9/2}$ (bottom) proton orbits in ^{102,110,120,130,170}Sn.

B. The neutrons in the Sn isotopes

Neutron orbit occupancies that result from the SLy4 model calculations are presented in Tables II–IV. They give the occupancies for orbits that are partially filled for each isotope of Sn. Orbits that have occupancies for all the nuclei in each table that is less than 0.03 are not listed.

Three of the isotopes have neutron orbits with complete occupancy. They are ^{100,132,176}Sn of which only ^{176}Sn is listed in the tables. The tables segment the mass range of the Sn isotopes with the neutron orbit occupancies for the set $^{102-130}$Sn given in Table II. That ranges between the two isotopes having closed shell occupancies in the SLy4 model. These lighter mass isotopes also have a neutron core basically the same as for the protons [Eq. (2)] though there is a small percentage breaking of full occupancy of the neutron $0g_{9/2}$ orbit as shown by the first line in Table II.

As neutrons are added pairwise to ^{100}Sn to reach mass 110, this model suggests that they primarily occupy the $1d_{5/2}$ orbit with some partial occupancy of both the $2s_{1/2}$ and $0g_{7/2}$ orbits. As mass then increases to reach ^{120}Sn, the latter two orbits increase in occupancy to $80\%-90\%$ while the $1d_{3/2}$ and $0h_{11/2}$ orbits fill to 68% and 20% closure respectively and at approximately the same rate. With the set of isotopes $^{122-132}$Sn, the major effect is in the filling of the $0h_{11/2}$ orbit. Higher shell states for all of these isotopes account for less than a percent of the neutron numbers. Of importance however, is that, with the SLy4 model, filling of the four important valence orbits is far from that one would guess with the simplest of shell schemes.

But once again the valence orbitals vary as the mass increases. That variation is illustrated in Fig. 6 where the four important valence orbital single particle densities are shown for three isotopes, ^{102,110,130}Sn. In this case we display just

TABLE II. Valence orbit occupancies from the SLy4 model for the isotopes $^{102-130}$Sn.

Orbit	102	104	106	108	110	112	114	116	118	120	122	124	126	128	130
$0g_{9/2}$	9.95	9.93	9.92	9.91	9.90	9.91	9.92	9.93	9.94	9.94	9.95	9.96	9.96	9.97	10.0
$1d_{5/2}$	1.65	3.21	4.44	4.97	5.22	5.39	5.54	5.66	5.75	5.82	5.86	5.89	5.92	5.95	5.97
$2s_{1/2}$	0.03	0.07	0.13	0.26	0.42	0.62	0.86	1.14	1.43	1.65	1.78	1.86	1.91	1.94	1.97
$1d_{3/2}$	0.06	0.11	0.18	0.32	0.49	0.71	1.01	1.45	2.07	2.73	3.22	3.52	3.70	3.82	3.92
$0g_{7/2}$	0.21	0.49	1.04	2.05	3.27	4.48	5.58	6.44	7.01	7.35	7.55	7.68	7.78	7.86	7.93
$0h_{11/2}$	0.07	0.14	0.23	0.39	0.56	0.73	0.92	1.19	1.62	2.31	3.41	4.86	6.51	8.27	10.1
$0i_{13/2}$		0.02	0.02	0.03	0.04	0.04	0.05	0.05	0.05	0.05	0.05	0.05	0.05	0.04	0.03
$1f_{7/2}$		0.01	0.02	0.02	0.03	0.03	0.04	0.04	0.04	0.04	0.05	0.05	0.05	0.04	0.03
$0h_{9/2}$		0.01	0.02	0.02	0.03	0.04	0.04	0.04	0.04	0.04	0.05	0.05	0.05	0.04	0.03

the changes wrought between $^{102-130}$Sn since for this range of nuclei essentially those four orbits are being filled with neutrons. Across this range of isotopes each valence orbit gradually extends in space. The related neutron densities then increase in size as neutrons are added to form a neutron skin. But such a skin is not due simply to an increase in neutron occupancy of orbits with high angular momentum. Each orbit's extension as the mass increases plays a role.

In Tables III and IV, respectively, the extra core neutron orbit occupancies for the isotopes $^{134-158}$Sn and $^{160-176}$Sn are given. For all of those isotopes the neutron core essentially has 62 neutrons. The 12 neutrons extra to the 50 in the configuration of Eq. (2) closes the $2s-1d$ shell.

The SLy4 model neutron orbit occupancies for the isotopes $^{134-158}$Sn given in Table III reveal that the $0g_{7/2}$ and $0h_{11/2}$ orbits are almost fully occupied. Thus in adding neutrons to reach ^{142}Sn, those neutrons almost all go into the $1f_{7/2}$ orbit, almost filling it completely. As neutrons are added thereafter, that $1f_{7/2}$ orbit occupancy decreases slightly before slowly regaining to almost full occupancy in ^{160}Sn. Furthermore, in changing from mass 144 to mass 162, the other orbits increase in occupancy, more or less at the same rate to result in 90% full for the $0h_{9/2}$ and $2p_{3/2}$ orbits, 70% full for the $1f_{5/2}$ and $2p_{1/2}$ orbits, and 30% occupation for the $0i_{13/2}$ orbit. Higher shells to these again account for less than 1% of the neutron numbers.

As before, as one moves across this range of isotopes, the individual orbit wave functions for the neutrons become more extended. That is shown in Fig. 7 wherein four (valence) orbit functions for ^{134,144,150,158}Sn are displayed. For ^{138}Sn, only the $1f_{7/2}$ wave function is shown (by the dot-dashed curve) since that is the only valence orbit of the four in that nucleus with a substantial neutron occupancy. However, for all four orbitals, the wave functions determined from the SLy4 calculations are portrayed by the solid, dashed, and dotted curves for ^{144}Sn, ^{150}Sn, and ^{158}Sn, respectively. Again these valence orbit wave functions extend to larger radii as the isotope mass increases, but now not as markedly as for the protons or neutron orbits for the lighter mass isotopes. It follows then that the buildup of neutron density at the nuclear surface is more influenced now by the increasing occupancies of these orbits.

The neutron orbit occupancies given by the SLy4 model for the heaviest Sn isotopes, masses 160–176, are given in

TABLE III. Valence orbit occupancies from the SLy4 model for the isotopes $^{134-158}$Sn.

Orbit	134	136	138	140	142	144	146	148	150	152	154	156	158
$0g_{7/2}$	8.00	8.00	8.00	8.00	8.00	7.98	7.97	7.97	7.97	7.97	7.97	7.97	7.97
$0h_{11/2}$	11.96	11.95	11.96	11.98	11.93	11.90	11.89	11.88	11.87	11.87	11.88	11.88	11.89
$1f_{7/2}$	1.82	3.67	5.57	7.62	7.98	7.40	7.41	7.44	7.47	7.52	7.57	7.62	7.67
$0h_{9/2}$	0.07	0.14	0.17	0.15	0.97	1.78	2.63	3.51	4.40	5.28	6.12	6.88	7.56
$0i_{13/2}$	0.05	0.09	0.11	0.07	0.37	0.63	0.88	1.13	1.39	1.66	1.96	2.31	2.71
$1f_{5/2}$	0.04	0.07	0.08	0.06	0.35	0.63	0.92	1.23	1.56	1.94	2.35	2.81	3.31
$2p_{3/2}$	0.03	0.05	0.07	0.09	0.73	1.31	1.80	2.19	2.51	2.77	3.00	3.19	3.36
$2p_{1/2}$		0.01	0.02	0.02	0.10	0.19	0.28	0.38	0.50	0.63	0.77	0.93	1.11
$1g_{9/2}$		0.01	0.01	0.03	0.03	0.04	0.05	0.06	0.07	0.08	0.09	0.09	0.10
$0j_{15/2}$		0.01	0.01	0.03	0.03	0.04	0.05	0.06	0.07	0.08	0.08	0.08	0.08
$0i_{11/2}$					0.02	0.03	0.04	0.05	0.06	0.06	0.07	0.07	0.07
$2d_{5/2}$						0.01	0.02	0.02	0.02	0.02	0.02	0.03	0.03
$1g_{7/2}$						0.01	0.02	0.02	0.03	0.03	0.03	0.03	0.03
$0k_{17/2}$						0.01	0.02	0.02	0.02	0.02	0.03	0.03	0.03

TABLE IV. Valence orbit occupancies from the SLy4 model for the isotopes $^{160-176}$Sn.

Orbit	160	162	164	166	168	170	172	174	176
$0g_{7/2}$	7.97	7.98	7.98	7.98	7.98	8.00	8.00	8.00	8.00
$0h_{11/2}$	11.90	11.91	11.92	11.93	11.94	11.96	11.97	11.98	12.00
$1f_{7/2}$	7.72	7.77	7.81	7.84	5.36	7.91	7.94	7.97	8.00
$0h_{9/2}$	8.13	8.59	8.96	9.24	9.46	9.63	9.77	9.89	10.00
$0i_{13/2}$	3.23	3.92	4.82	5.98	7.35	8.87	10.50	12.21	14.00
$1f_{5/2}$	3.82	4.32	4.76	5.10	5.36	5.56	5.72	5.87	6.00
$2p_{3/2}$	3.50	3.62	3.71	3.78	3.84	3.88	3.92	3.96	4.00
$2p_{1/2}$	1.30	1.48	1.61	1.73	1.81	1.87	1.92	1.96	2.00
$1g_{9/2}$	0.10	0.10	0.10	0.10	0.10	0.09	0.07	0.04	—
$0j_{15/2}$	0.08	0.08	0.08	0.08	0.08	0.07	0.05	0.03	—
$0i_{11/2}$	0.07	0.07	0.07	0.07	0.07	0.06	0.05	0.03	—
$2d_{5/2}$	0.03	0.03	0.02	0.02	0.02	0.02	0.02	—	—
$1g_{7/2}$	0.03	0.03	0.03	0.03	0.03	0.02	0.02	0.01	—
$0k_{17/2}$	0.03	0.03	0.02	0.02	0.02	0.02	0.01	—	—

Table IV. Those trend to a complete shell occupancy for ^{176}Sn. The most obvious change in occupancy over this set of nuclei is that of the $0i_{13/2}$ orbit (from 3.23 to 14 neutrons). Again the higher orbits are sparsely occupied, and in fact any such occupancy decreases until ^{176}Sn adopts the closed shell character.

The wave functions for the valence orbitals of importance for the heaviest Sn isotopes are displayed in Fig. 8 where the solid curves are the functions specified for ^{160}Sn and the dashed curves show those for ^{176}Sn.

IV. SCATTERING FROM HYDROGEN–GEDANKEN RESULTS

We have used the canonical single particle wave functions for all of the Sn isotopes to fold an effective NN interaction and thus generate optical potentials for use in modified versions of the scattering program DWBA98 [23]. Those optical potentials are complex and nonlocal since they can be written in coordinate space with $\boldsymbol{r}_{12}=\boldsymbol{r}_1-\boldsymbol{r}_2$, as

$$U(\boldsymbol{r}_1,\boldsymbol{r}_2;E) = U_D(\boldsymbol{r}_1;E)\,\delta(\boldsymbol{r}_{12}) + U_E(\boldsymbol{r}_1,\boldsymbol{r}_2;E), \tag{3}$$

where the direct U_D and nonlocal exchange U_E terms are

$$U_D = \sum_n \zeta_n \left(\int \varphi_n^*(\boldsymbol{s}) v_D(\boldsymbol{r}_{1s}) \varphi_n(\boldsymbol{s}) d\boldsymbol{s} \right)$$

$$U_E = \sum_n \zeta_n [\varphi_n^*(\boldsymbol{r}_1) v_{Ex}(\boldsymbol{r}_{12}) \varphi_n(\boldsymbol{r}_2)], \tag{4}$$

where v_D and v_{Ex} are combinations of the components of the effective NN interactions, ζ_n are ground state occupancies of nucleons within the shell "n," and $\varphi_n(\boldsymbol{s})$ are nucleon single particle states. The occupancies are the particular OBDME:

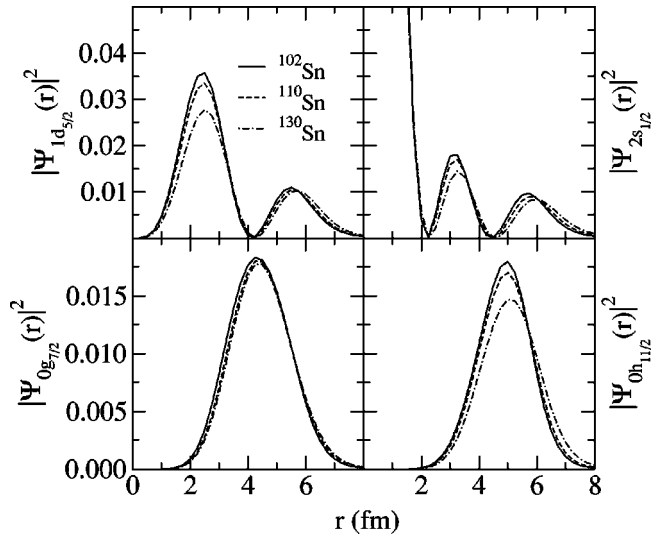

FIG. 6. The moduli square of the radial functions for four neutron orbits in ^{102,110,130}Sn.

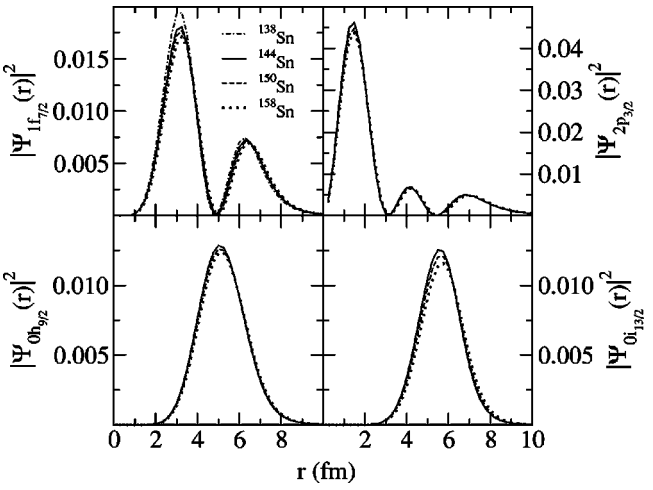

FIG. 7. Radial wave functions for four neutron orbits in ^{134,144,150,158}Sn.

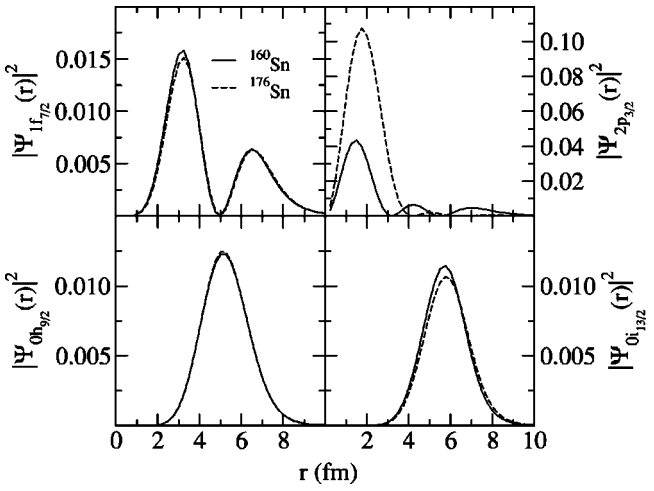

FIG. 8. Radial wave functions for four neutron orbits in ^{160}Sn and ^{176}Sn.

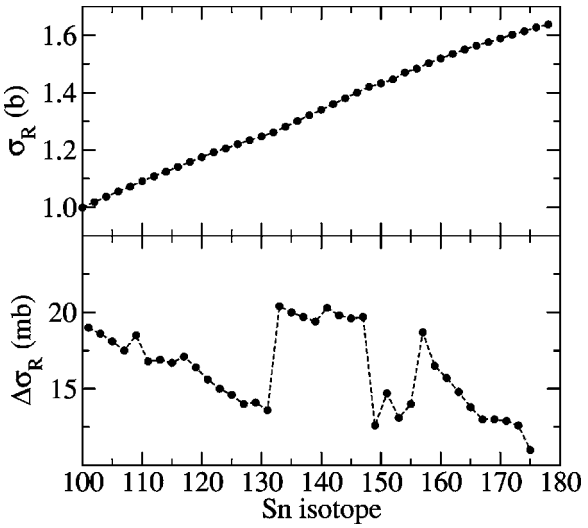

FIG. 9. The reaction cross sections for 200 MeV proton scattering from the even mass Sn isotopes (top) and the differences between those total reaction cross sections for adjacent isotopes (bottom).

$$\zeta_n = \langle \Psi_{J=0}(1,2,\cdots,A) \| [a_n^\dagger \otimes a_n]^{I=0} \| \Psi_{J=0}(1,2,\cdots,A) \rangle, \tag{5}$$

where the operator is the usual particle-hole operator. Note some models may allow non-Hartree components in the A-particle wave functions (a change of principal quantum number) which will then allow nondiagonal zero spin state expectations in Eq. (5). They give additional contributions to the optical potentials, as do elements with $J \neq 0$ when one considers odd mass or special nuclei such as ^{6}Li. However, none such occur with the model structures we have chosen for the Sn isotopes. All details and the prescription of solution of the associated nonlocal Schrödinger equations are given in the recent review [8]. The results to be discussed herein have been obtained by solving the actual nonlocal Schrödinger equations defined with potentials as given by Eq. (3). For the present calculations, the effective NN interactions have been defined by their mapping to the Brueckner-Bethe-Goldstone *g* matrices of the BonnB NN interaction [28].

We consider the elastic scattering of 200 MeV protons from each of the even mass Sn isotopes ($A=100-176$). By inverse kinematics the cross sections we determine are also those for the scattering of 200 A MeV Sn ions from hydrogen; some of which can be, or may soon be, obtained in sufficient numbers to form a radioactive ion beam for experiment. The choice of 200 MeV was made, not only because the effective force at this energy has been used in many successful predictions of actual scattering data from stable nuclei [8] but also data at that energy from ^{208}Pb gave a clear signature of its neutron density profile [9].

Possibly first measurements with such exotic nuclear projectiles may be of the total reaction cross sections and the SLy4 model predictions for those are shown in the top panel of Fig 9. There is a distinct mass trend in those results so that total reaction cross section gradually increases with isotope mass from ~1 b to 1.63 b for ^{170}Sn. The sums that define the reaction cross sections are dominated by the large partial wave scattering amplitudes [29]. Also, at much higher energies, those sums are known to equate to the geometric cross section for each nucleus. So reaction cross section values reflect a bulk character of the structure of each nucleus and values of the total reaction cross sections may then be the first obvious evidence of the propriety of any chosen model for the structure of the isotopes. If any can be measured accurately, the differences between the total reaction cross sections between adjacent even mass isotopes may also be test of the structure models since, as portrayed in the bottom segment of Fig. 9, there is a noticeable variation of many mb predicted. Note that the differences show a trend to smaller values with increasing mass save for a "quantum" jump when the neutron number is 82, and for some uniqueness with masses 150–156, but any such clear variation will require an accuracy of measurement of a percent or two. Nonetheless, the actual value first, and the trend of differences second, may signify propriety of the structures chosen to describe the isotopes.

There appears to be little difference between the cross sections found using the SkP and the SLy4 forces to give the ground state structures. This is shown for a select set of Sn isotopes in Fig. 10. The differential cross sections for 200 MeV proton scattering from ^{100,110,120,130}Sn are shown in the top panel with each scaled by factors of 1, 2, 4, and 8 to distinguish them from one another more clearly. The ratio to Rutherford scattering for these same nuclei and at 200 MeV are displayed in the bottom panel of this figure. The solid (dashed) curves were obtained by using the structure found with the SkP (SLy4) force. On this scale there is little to distinguish between the alternate model results. But the two structure models do predict cross sections that differ in detail and such is shown in Fig. 11 for the set of isotopes ^{100,110,120,130,140,150,160}Sn. Therein the percentage difference,

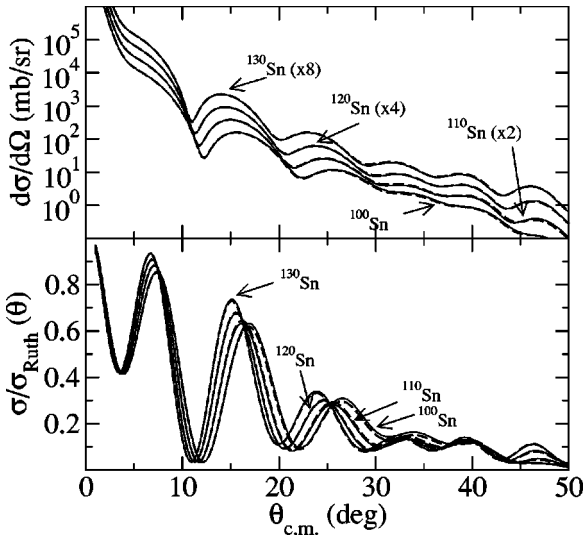

FIG. 10. The cross sections from 200 MeV proton scattering with select Sn isotopes. The differential cross sections are shown in the top panel while the ratios to Rutherford results are displayed in the bottom panel.

$$\%\ \text{difference} = \left[\frac{d\sigma_{\text{SkP}}}{d\Omega} - \frac{d\sigma_{\text{SLy4}}}{d\Omega}\right] \Bigg/ \left|\frac{d\sigma_{\text{SkP}}}{d\Omega}\right| \times 100, \tag{6}$$

is plotted for each nucleus as identified. Differences can be large (20%) as with ^{150}Sn coinciding with cross ection magnitudes of a few mb/sr at scattering angles $\sim 30° - 40°$. That coincides with momentum transfer values of $\sim 1-2$ fm^{-1} and are values which might be distinguished by measurement. In the main however, the model differences characteristically are 5%–10%, so that at scattering angles of 20° where predicted cross sections (for 200 MeV) are about 20 mb/sr, the

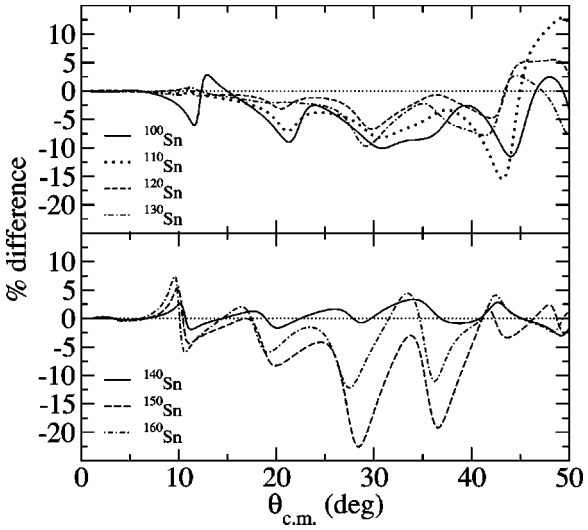

FIG. 11. Percentage differences between differential cross sections for 200 MeV proton scattering which were calculated using the two structure model densities.

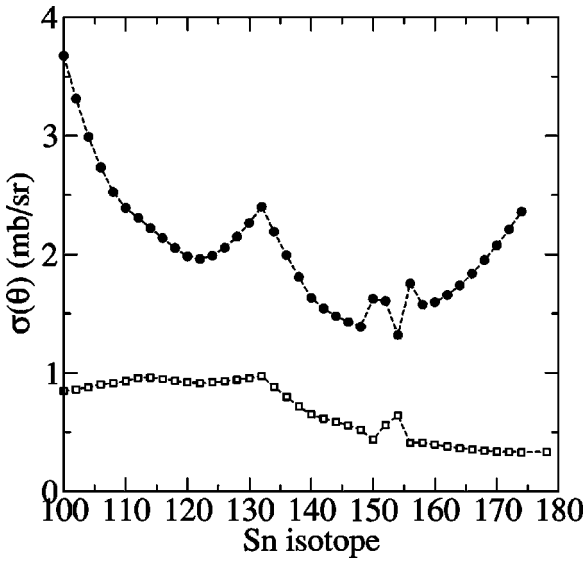

FIG. 12. The differential cross section values at 30° (circles) and 40° (squares) scattering for all even mass Sn isotopes as evaluated using the SLy4 model of their structure.

difference between the model predictions would be about a mb/sr. For larger angle results, where the cross section magnitude is of the order of a mb/sr the differences, $\sim 0.05-0.1$ mb/sr may not exceed experimental uncertainties. Nonetheless there is a progression in these cross section differences found using the sets of matter densities given by the SkP and SLy4 structure models as one increases the isotope mass and when compared with data, such might suggest preference for one model of structure over the other; presupposing of course that one is indeed a better description of reality. To illustrate this further, in Fig. 12 we show the cross section values at 30° and 40° scattering that result from using the SLy4 structure model to form *g*-folding optical potentials. The momentum transfers for these scattering angles are ~ 1.5 and ~ 2 fm^{-1}, respectively. At these momentum transfer values, clearly the variation of the structure details with mass have noticeable effect. There is some evidence for a more packed neutron distribution in the structures at neutron number 82 and some evidence of surface orbit variations with neutron numbers 100, 102, and 104. The latter, however, may simply be an idiosyncrasy of the model calculations. Thus, and as found in a study of scattering from ^{208}Pb [9], the neutron distribution through the nuclear surface in particular, reflects strongly in the calculated values for elastic scattering cross sections for momentum transfers $1-2.5$ fm^{-1} with cross section values ~ 1 mb/sr.

Other properties of the cross sections reflect possible measurable trends. In Fig. 13 diverse variations with mass in the entire set of isotopes are shown. Such are quantities from scattering having analogies with the bulk nuclear properties determined previously from the mean-field matter densities [6]. In the top panel the variations with mass of magnitudes of select (low momentum) peaks in the calculated cross sections are shown. The first obvious peak in the differential cross section is displayed by the filled circles. That changes markedly as one progresses from proton to neutron drip

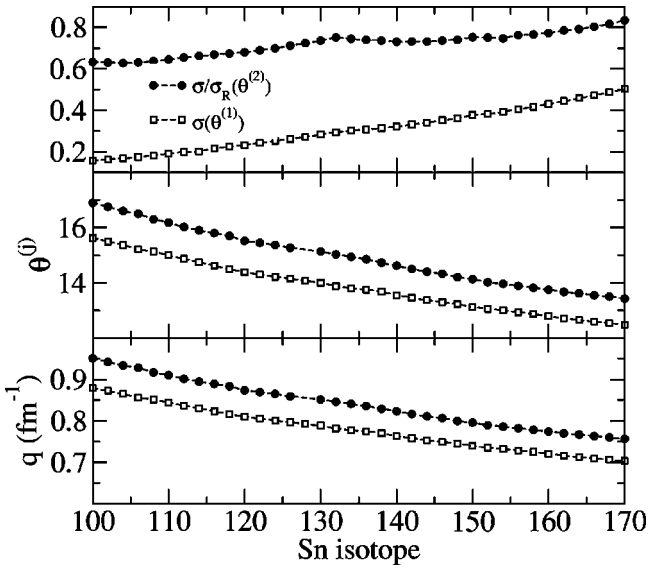

FIG. 13. Some low momentum transfer characteristics of 200 MeV proton scattering from the 110–170 even mass Sn isotopes. In the top panel, the ratio to Rutherford cross section values for scattering angles $\theta_{(2)}$ are denoted by the (filled) circles while the differential cross section values for $\theta_{(1)}$ are depicted by (open) squares. The values of the angles for each target are shown in the central, and the corresponding momentum transfers in the bottom, panels. The subscripts to the angles designate those at which the first and second peaks occur in the relevant cross sections.

lines, from the value of ~150 mb/sr for ^{100}Sn to a value of ~500 mb/sr for ^{170}Sn as shown and on to ~540 mb/sr for ^{176}Sn. As with the total reaction cross section results this variation would be a measurable effect in future scattering experiments, and one that may be an easier characteristic to define than the higher momentum properties we described earlier. The *y*-axis in this case is to be read as b/sr. In the top panel we also display the values of the ratio to Rutherford cross sections found at the scattering angles corresponding to the second peak in those ratios. They are portrayed by the opaque squares with the *y*-axis now in dimensionless units. Again there is a smooth measurable effect with mass, both in the magnitude of that second ratio to Rutherford peak as well as with the angles at which that peak occurs. We have designated these trends as low momentum properties as specified by the prescriptions. The particular values involved are shown in the middle and bottom panels of this figure. In the middle panel the center of mass scattering angles at which the differential cross sections have their first definite peak are shown by the filled circles while those at which the ratio to Rutherford cross sections have their second peak are displayed once again by the opaque squares. With increasing mass, and for all the isotopes, the first prominent peak of the differential cross sections move inward to smaller values of momentum transfer. Over the entire range, the momentum transfer value at which the first peak occurs changes from 0.88 fm^{-1} in ^{100}Sn to 0.7 fm^{-1} in ^{170}Sn.

V. COMPARISON WITH DATA

There have been many experimental studies of proton scattering from Sn isotopes. Our literature search on those gave the listing as shown in Table V. The proton energy was restricted to the range 16–200 MeV; a range for which we felt most comfortable about using the *g*-folding method of defining optical potentials, and for which range we are confident about the effective NN interactions we have defined [8].

From that list we have chosen for analysis, some of the data taken at 39.8, 49.35, 65.0, and 200.0 MeV. A complete analysis of all of the available data will be made and reported in some fashion subsequently. In all of the figures to be shown, unless otherwise stated, the calculated results were obtained from optical potentials formed by folding a Melbourne effective NN interaction [8] for the relevant incident energy, with the OBDME and single particle wave functions determined by the SLy4 model of structure for each and every isotope of Sn. The DWBA98 program [23] was used to perform the folding and to find solutions of the relevant Schrödinger equations.

The first result we show is of the scattering of 39.8 MeV protons from ^{120}Sn. In Fig. 14, our calculated cross section as

TABLE V. Selected list of references to data and analyses of data from proton elastic scattering from Sn isotopes.

Energy	Isotopes	References
16.0	116, 120, 124	[31], [32], [33]
20.4	116, 118, 120, 122, 124	[34]
24.5	116, 118, 120, 124	[35], [36], [34]
30.3	112, 114, 116, 118, 120, 122, 124	[37], [38], [39], [40], [41]
39.6	116, 118, 120, 122, 124	[30], [42], [43]
49.35	112, 114, 118, 120, 124	[32]
61.4–65	118, 120	[44], [45], [46]
100.0–104.0	120	[43], [47], [48], [49]
133.8	116	[50]
156.0–160.0	116, 118, 120	[51], [52]
200	120	[53]

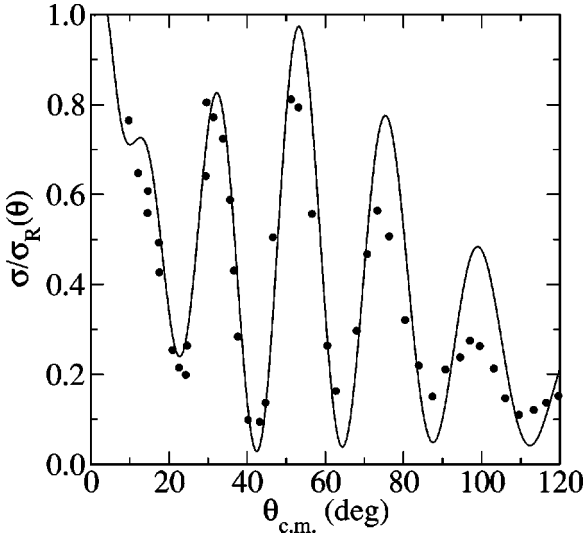

FIG. 14. The cross section as a ratio to Rutherford for the scattering of 39.8 MeV protons from ^{120}Sn. The data (Ref. [30]) are compared with the result of a calculation made using the *g*-folding optical potential as described in the text.

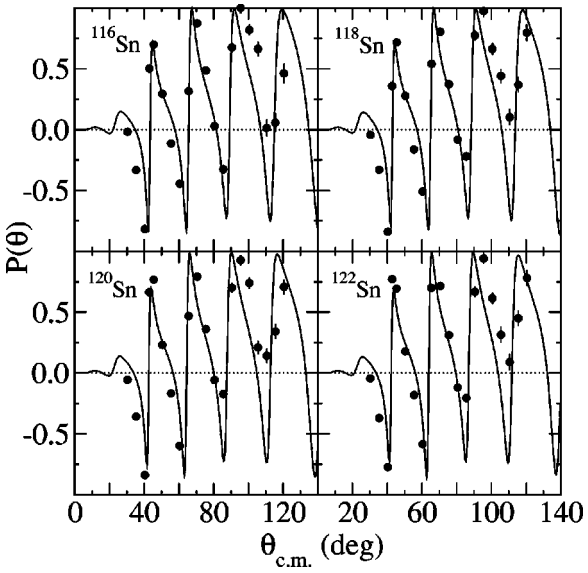

FIG. 16. Polarizations for the elastic scattering of 39.8 MeV protons from ^{116,118,120,122}Sn. The data [42] are compared with calculated results as found using the *g*-folding model.

a ratio to Rutherford scattering is compared with data [30]. Clearly the trend of the data is reproduced by the *g*-folding optical potential calculation and some details are also well matched. Similar quality of matching to data for the set of even mass isotopes, $^{116-124}$Sn, is revealed in Fig. 15. The data [42] for the sequence of isotopes 116–124 are displayed by down filled triangles, by up (opaque) triangles, by filled diamonds, by opaque squares, and by filled circles, respectively. For the same sequence the results of our calculations are displayed by the double dot-dashed, the single dot-dashed, the dashed, the dotted, and the solid curves, respectively. With all data collected in this figure, and the spread of the calculated values for the five isotopes giving a band of predictions, the trend of data is well reproduced by the predicted values, at least to 90°. The quality of fit to individual polarizations is presented in Fig. 16. The maxima (positive and negative) values are in good agreement with the characteristic shapes between the sharp rises in values (from negative to positive) being predicted. The variations between data and calculated values are not great and it seems within the realm of possibility that small changes to the chosen structure model can improve the agreement. Such is also the conclusion we may draw from the comparison of results with data

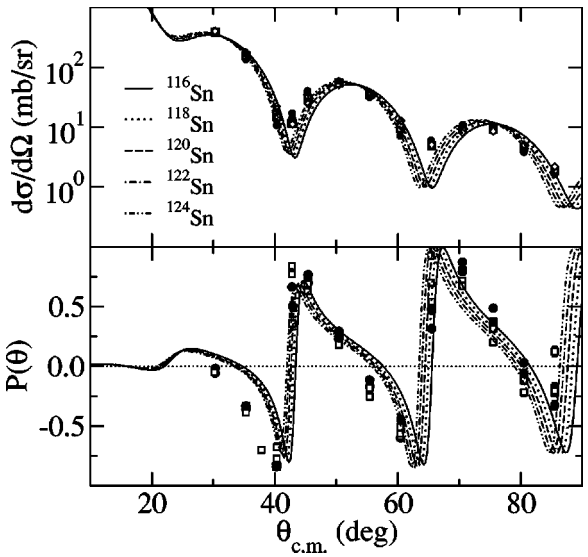

FIG. 15. The differential cross sections (top) and polarizations (bottom) for the elastic scattering of 39.8 MeV protons from ^{116,118,120,122,124}Sn with symbols giving data [42].

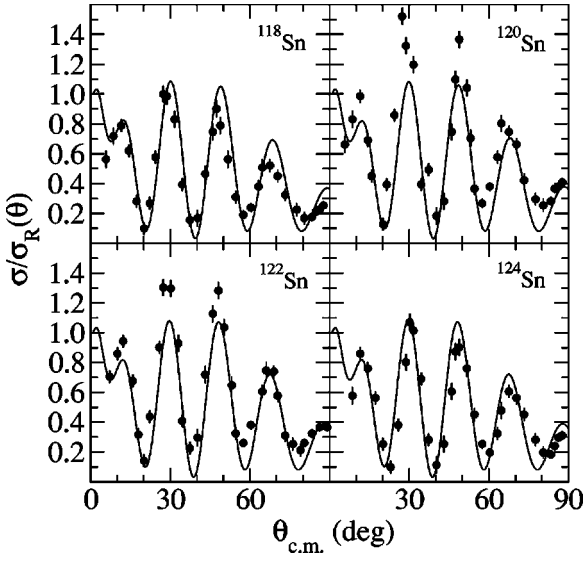

FIG. 17. The cross section as a ratio to Rutherford for the scattering of 49.35 MeV protons from ^{118,120,122,124}Sn. The data [32] are compared with the results of calculations made using *g*-folding optical potentials.

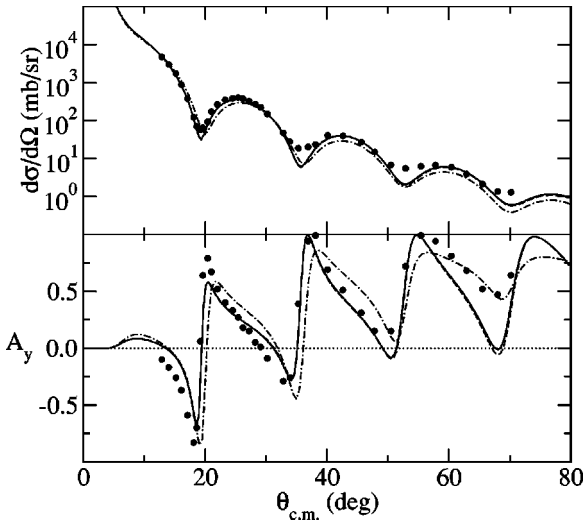

FIG. 18. The differential cross sections (top) and analyzing powers (bottom) for the elastic scattering of 65 MeV protons from ^{118}Sn. The data [54] are compared to the results of the calculations made using the SLy4 (solid line), SkP (dashed line), and HO (dot-dashed line) models.

taken at 49.3 MeV. Cross sections as ratios to Rutherford are shown in Fig. 17. The data [32] now display a variation with target mass that is not readily mapped by our calculated results. With ^{122,124}Sn, the peak values of the ratios exceed our predictions by 30%–40%. However, the trend of data as well as a number of specific details are well matched and we consider then that the results confirm credibility of the SLy4 structure.

Finally, we show results found for the elastic scattering of 65 MeV protons from ^{118}Sn and of 200 MeV protons from

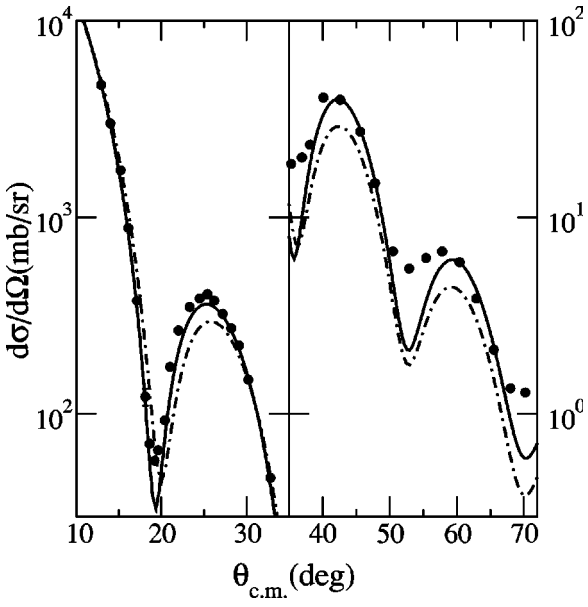

FIG. 19. The differential cross sections for the elastic scattering of 65 MeV protons from ^{118}Sn. The data [54] are compared to the results of the calculations made using the SLy4 (solid line) and HO (dot-dashed line) models.

^{120}Sn. At those energies many successful predictions have been made of cross sections for proton scattering from stable nuclei [8]. Included in that set were predictions of scattering from two Sn isotopes of the set considered herein. Those Sn cross-section calculations of the past were made using single particle oscillator (HO) wave functions determined with an oscillator length given by an $A^{1/6}$ rule, i.e., values of 2.215 and 2.221 fm were used for ^{118}Sn and ^{120}Sn, respectively. In the following figures, we display cross sections found using those HO model densities by the dot-dashed curves. Those results found using the SLy4 and SkP model densities are shown by the solid and dashed curves respectively.

In Fig. 18 the differential cross sections and analyzing powers for the elastic scattering of 65 MeV protons from ^{118}Sn [54], are compared with our predictions. In the case of the differential cross section, there is little difference ($\sim$1%) between those found using the SLy4 and SkP structures but both are distinctly better than the cross sections found by using HO functions. This is emphasized in the next figure. However, while the SLy4 (and SkP) model results are in good agreement generally with the structure and magnitude of the data, the calculated minima are too deep; a feature indicative of the need for more absorption. The 65 MeV force we have used gave excellent fits to 65 MeV data from many nuclei [8], including depth of minima. Perhaps this feature may be due to processes beyond the Born limit inherent in use of the DWBA98 code.

The preference for the SLy4 (SkP) model as well as other evidence for increased absorption, is also evident with the total reaction cross section. The SLy4 model predicts 1.48 b for this property while the HO calculation yields 1.41 b. The measured value [55] is 1.535 ± 0.047 b but it is with the analyzing power at 65 MeV that the SLy4 (SkP) densities give a significantly better result in comparison to the HO model. While the HO result is a fair reproduction of the data structure, the SLy4 (SkP) model result gives not only the correct location of the maxima and minima but also shows the overall trend, seen in the data, of increasingly positive values with increasing angle. They also depict best the marked asymmetric shape of each peak structure of the data. It has been noted [8] that the location and gradient of variation from most negative to most positive values in analyzing powers correlates quite well with the distribution of nucleons through the nuclear surface.

To emphasize the disparity with the cross sections shown in Fig. 18, in Fig. 19 we show the cross sections in larger scale. The error bars on the data remain within the size of the dots shown with values usually less than 1% of the quoted magnitudes. The curves depict the results obtained with the SLy4 model (solid) and the HO model (dot-dashed) and the results are split into two scattering angle ranges as indicated. The HO model results give a sharper decrease with momentum transfer than do either the actual data or the SLy4 model cross sections, so that the HO model cross section is too large at angles forward of 20° and too small for all but two larger scattering angles. The SLy4 model results on the other hand have quite good trend with momentum transfer, being a quite excellent fit to the data forward of 20° and reproducing the position and peak magnitudes of data for larger angles. As noted before, it is with the values of the minima that there

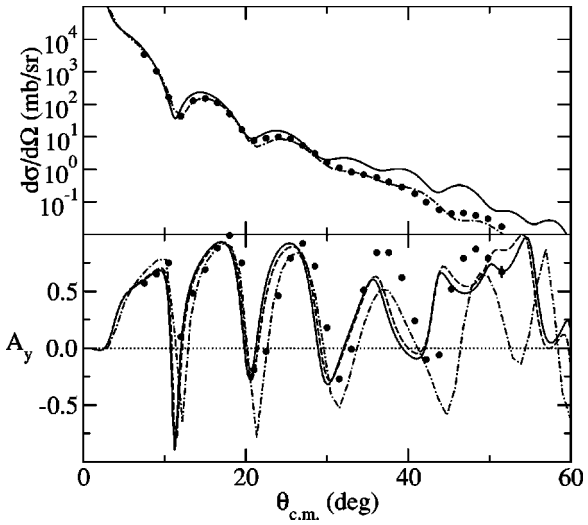

FIG. 20. The differential cross sections (top) and analyzing powers (bottom) for the elastic scattering of 200 MeV protons from ^{120}Sn. The data [56] are compared to the results of the calculations made. The curves are as for Fig. 18. The SkP result is not given for the cross section as it is indistinguishable from the SLy4 result.

is a mismatch. The position of the minima are well reproduced.

The 200 MeV scattering results from ^{120}Sn are an exception to the pattern so far established. In this case it is the HO model rather than the SLy4 one which reproduces data well. The differential cross sections and analyzing powers are shown in Fig. 20 from which it is clearly evident that the HO model tracks the measured data [56] well for all angles shown. The SLy4 model result is not as good, though it agrees with the forward angle ($<30°$) scattering data well enough. The SkP model result is indistinguishable from the SLy4 one on this scale. The actual differences in cross section are less than a percent at most scattering angles. Both the SLy4 and SkP models thus overestimate the cross section and predict some structure not seen in the data for larger scattering angles. Such discrepancies have been noted in other circumstances, notably in a comparative study [9] of model structures for ^{208}Pb and in identifying ^{6}He and ^{11}Li as nuclei with extended neutron distributions (neutron halos) [57,58]. Furthermore, RIA model results for 200 and 295 MeV scattering [22] find predictions that are larger, and have more structure, than the data for scattering angles greater than $\sim 15°$. It is also of note that the 200 MeV data at scattering angles $>25°$ are smoothly decreasing and so quite unlike the equivalent data at lower energies. However, note that the "problematic" data in this 200 MeV cross section has a magnitude <1 mb/sr; cross section magnitudes for which we have lessened confidence that processes other than inherently considered within the *g*-folding method can be neglected.

As with the differential cross section results, our predictions for the analyzing powers (shown in the bottom half of Fig. 20) are good but there is room for improvement. The asymmetry seen with the 65 MeV data is less severe at this higher energy but, of course, there are more peaks within the scattering angle range shown. Both features are evident in the HO and SLy4 calculations without the exact angular structures in the data being reproduced. The SLy4 and SkP results do match the observed peak magnitudes and valley depths very well and the two densities yield slight differences in the spin measurable.

VI. CONCLUSIONS

We have made predictions of the observables of the elastic scattering of 200 MeV protons from the even–even isotopes of Sn from ^{100}Sn to ^{176}Sn taking the structure of the isotopes from a Hartree-Fock-Bogoliubov model using the Skyrme interaction. Two parameterizations of the Skyrme force have been used. The matter densities obtained from those models show consistent trends. As mass increases from $A=100-176$, the neutron central density increases and a neutron skin emerges. Also, as the proton number is fixed, the addition of neutrons not only increases the volume but also engenders a dilution of the proton distribution.

The changes in the nucleon densities reflect in the predictions made for the differential cross sections of 200 MeV proton elastic scattering. As the neutron number increases, the first three minima tend to lower momentum transfers and the intervening first maximum becomes more pronounced. That effect as the neutron skin becomes more manifest is large enough to be distinguishable in experiment.

For the set of isotopes $^{116-124}$Sn cross sections, polarizations, and analyzing powers in proton elastic scattering have been measured at various energies. Most of that data compare well with predictions from *g*-folding optical potential calculations when those potentials are defined by folding with the SLy4 model of the structure of the isotopes. However there is little difference between those results and ones obtained by using the SkP model but both models give results that are much better, usually, than those found by using a naive oscillator model for the structure of the isotopes. The fact that there are marked differences between the HO and SLy4 model predictions signifies the value of using proton elastic scattering data in testing model specifications of the ground states of nuclei. The 200 MeV results for the scattering from ^{120}Sn is exceptional. Bearing in mind the effects observed in a recent study [9] of proton scattering from ^{208}Pb, perhaps the neutron matter distribution just within the nuclear surface as determined by either of the calculations needs slight variation.

Overall we have shown that the Skyrme-Hartree-Fock-Bogoliubov models give a very reasonable description of the ground states of the stable Sn isotopes and, assuming they do so for the other masses, then the cross sections for scattering from hydrogen will distinguish the progressive addition of neutrons to form the isotopes.

It is hoped that, with the proposed new generation of radioactive beam facilities, data for the elastic scattering of heavy neutron-rich nuclei from hydrogen will be obtained at select momentum transfer values where our predictions of cross sections are sensitive to the major details in the neutron density. We contend that such experiments and analyses serve as an important test of the models being developed to

describe exotic nuclei and which inherently give distinctive differences in features such as the neutron rms value.

ACKNOWLEDGMENTS

This work was supported by a grant from the Australian Research Council and by the Polish Committee for Scientific Research (KBN) under Contract No. 5 P03B 014 21. We also gratefully acknowledge the assistance of Dirk van der Knijff of the Advanced Research Computing Group, Information Division, University of Melbourne for use of the high performance computers of that Group to find all of the results displayed.

[1] P. Hansen, A. Jensen, and B. Jonson, Annu. Rev. Nucl. Part. Sci. **45**, 591 (1995).
[2] E. Roeckl, Rep. Prog. Phys. **55**, 1661 (1992).
[3] A. Mueller and B. Sherrill, Annu. Rev. Nucl. Part. Sci. **43**, 529 (1993).
[4] K. Riisager, Rev. Mod. Phys. **66**, 1105 (1994).
[5] J. Dobaczewski and W. Nazarewicz, Philos. Trans. R. Soc. London, Ser. A **356**, 2007 (1998).
[6] S. Mizutori, J. Dobaczewski, G. Lalazissis, W. Nazarewicz, and P.-G. Reinhard, Phys. Rev. C **61**, 044326 (2000).
[7] J. Dobaczewski, I. Hamamoto, W. Nazarewicz, and J. Sheikh, Phys. Rev. Lett. **72**, 981 (1994).
[8] K. Amos, P. J. Dortmans, H. V. von Geramb, S. Karataglidis, and J. Raynal, Adv. Nucl. Phys. **25**, 275 (2000).
[9] S. Karataglidis, K. Amos, B. A. Brown, and P. K. Deb, Phys. Rev. C **65**, 044306 (2002).
[10] B. D. Serot and J. D. Walecka, Adv. Nucl. Phys. **16**, 1 (1986).
[11] L. S. Celenza and C. M. Shakin, *Relativistic Nuclear Problem* (World Scientific, Singapore, 1986).
[12] B. A. Nikolaus, T. Hoch, and D. G. Madland, Phys. Rev. C **46**, 1757 (1992).
[13] P. Ring, Prog. Part. Nucl. Phys. **37**, 193 (1996).
[14] T. Bürvenich, D. G. Madland, J. A. Maruhn, and P.-G. Reinhard, Phys. Rev. C **65**, 044308 (2002).
[15] P. Ring and P. Schuck, *The Nuclear Many-Body Problem* (Springer, Berlin, 1980).
[16] B. A. Brown, Phys. Rev. Lett. **85**, 5296 (2000).
[17] J. Dobaczewski, W. Nazarewicz, and P.-G. Reinhard, Nucl. Phys. **A693**, 361 (2001).
[18] M. Bender, P.-H. Heenen, and P.-G. Reinhard, Rev. Mod. Phys. **75**, 121 (2003).
[19] B. C. Clark, L. J. Kerr, and S. Hama, Phys. Rev. C **67**, 054605 (2003).
[20] P. K. Deb, K. Amos, S. Karataglidis, M. B. Chadwick, and D. G. Madland, Phys. Rev. Lett. **86**, 3248 (2001).
[21] H. Takeda *et al.*, in *Proceedings of the Kyudai-RCNP International Symposium;Nuclear Many-Body and Medium Effects in Nuclear Interactions and Reactions*, edited by K. Hatanaka, T. Noro, K. Sagara, H. Sakaguchi, and H. Sakai (World Scientific, Fukuoka, Japan, 2003), p. 269.
[22] T. Terashima *et al.* (2003), in RCNP Annual Report (unpublished).
[23] J. Raynal (1998), computer program DWBA98, NEA 1209/05.
[24] J. Dobaczewski, H. Flocard, and J. Treiner, Nucl. Phys. **A422**, 103 (1984).
[25] J. Dobaczewski, W. Nazarewicz, T. Werner, J.-F. Berger, C. Chinn, and J. Dechargé, Phys. Rev. C **53**, 2809 (1996).
[26] E. Chabanat, P. Bonche, P. Haensel, J. Meyer, and F. Schaeffer, Nucl. Phys. **A627**, 710 (1997).
[27] J. Dobaczewski, W. Nazarewicz, and T. Werner, Phys. Scr., T **56**, 15 (1995).
[28] R. Machleidt, K. Holinde, and C. Elster, Phys. Rep. **149**, 1 (1987).
[29] P. K. Deb and K. Amos, Phys. Rev. C **66**, 024604 (2002).
[30] M. P. Fricke, E. E. Gross, B. J. Morton, and A. Zucker, Phys. Rev. **156**, 1207 (1967).
[31] R. N. Boyd, J. Fenton, M. Williams, T. Kruse, and W. Savin, Nucl. Phys. **A162**, 497 (1971).
[32] G. S. Mani, D. T. Jones, and D. Jacques, Nucl. Phys. **A165**, 384 (1971).
[33] D. J. Abbott, T. B. Clegg, and J. P. Delaroche, Phys. Rev. C **35**, 2028 (1987).
[34] S. D. Wassenaar *et al.*, J. Phys. G **15**, 181 (1989).
[35] A. Tarats, J.-L. Escudie, and I. Brissaud, Nucl. Phys. **A362**, 128 (1981).
[36] N. Pingzhi, Chin. J. Nucl. Phys. **7**, 313 (1985).
[37] R. M. Craig, J. C. Dore, G. W. Greenlees, L. S. Lilley, and J. Lowe, Nucl. Phys. **58**, 515 (1964).
[38] G. W. Greenlees, V. Hnidzo, O. Karban, J. Lowe, and W. Makofske, Phys. Rev. C **2**, 1063 (1970).
[39] V. Hnidzo and J. Lowe, Phys. Lett. **35B**, 311 (1971).
[40] A. G. Hardacre *et al.*, Nucl. Phys. **A173**, 436 (1971).
[41] R. W. Manweiler, Nucl. Phys. **A240**, 373 (1975).
[42] R. N. Boyd and G. W. Greenlees, Phys. Rev. **176**, 1394 (1968).
[43] P. Haensel, Nucl. Phys. **A245**, 29 (1975).
[44] C. B. Fulmer, J. B. Ball, A. Scott, and M. L. Whitten, Phys. Rev. **181**, 1565 (1969).
[45] F. Hachenburg, H. C. Chiang, and J. Hufner, Phys. Lett. **97B**, 183 (1980).
[46] Z.-Y. Ma, P. Zhu, Y.-Q. Gu, and Y.-Z. Zhuo, Nucl. Phys. **A490**, 619 (1988).
[47] K. Kwiatowski and N. S. Wall, Nucl. Phys. **A301**, 349 (1978).
[48] P. Schwandt *et al.*, Phys. Rev. C **26**, 55 (1982).
[49] S. Kailas *et al.*, Phys. Rev. C **29**, 2075 (1984).
[50] S. Y. van der Werf *et al.*, Phys. Rev. C **36**, 1796 (1987).
[51] V. Comparat, R. Frascaria, N. Marty, M. Morlet, and A. Willis, Nucl. Phys. **A221**, 403 (1974).
[52] D. R. Sarker, H. Kabir, M. A. Rahman, and H. M. S. Gupta, Int. J. Mod. Phys. E **11**, 403 (2002).
[53] K. Kaki and H. Toki, Nucl. Phys. **A696**, 452 (2001).
[54] M. Yosoi *et al.*, in RCNP Annual Report, 1985, p. 4.
[55] A. Ingemarsson *et al.*, Nucl. Phys. **A653**, 341 (1999).
[56] H. Sakaguchi *et al.*, in RCNP Annual Report, 1993, p. 4.
[57] A. Lagoyannis *et al.*, Phys. Lett. B **518**, 27 (2001).
[58] S. Stepantsov *et al.*, Phys. Lett. B **542**, 35 (2002).